August 2009
Technical Memorandum: UCPRC-TM-2008-16

Mn/ROAD Case Study Using *CalBack* and *CalME*

Author:
Bor-Wen Tsai and Rongzong Wu

Partnered Pavement Research Program (PPRC) Contract Strategic Plan Element 4.1:
Development of Mechanistic-Empirical Design Method

PREPARED FOR:

California Department of Transportation
Division of Research and Innovation
Office of Roadway Research

PREPARED BY:

University of California
Pavement Research Center
UC Davis, UC Berkeley

DOCUMENT RETRIEVAL PAGE			Technical Memorandum: UCPRC-TM-2008-16
Title: Mn/ROAD Case Study Using *CalBack* and *CalME*			
Author: B. Tsai and R. Wu			
Prepared for: California Department of Transportation Division of Research and Innovation Office of Roadway Research	**FHWA No.:** CA111201a	**Date Work Submitted:** March 31, 2010	**Date:** August 2009
Strategic Plan No: 4.1	**Status:** Stage 6, final draft		**Version No:** 1

Abstract: This study demonstrates how the software programs *CalBack* and *CalME* were used to predict the in-situ pavement performance of two test sections at the Minnesota Road Research Project (Mn/ROAD). The study demonstrates the benefits of using *CalBack* to backcalculate changes in layer moduli from deflection data; the resulting data show the influence of freeze/thaw and seasonal changes of subgrade stiffness; the confining effects of overlying layers; and the hardening/aging effects of time on the hot-mix asphalt (HMA).

Data from the comprehensive Mn/ROAD database were used to run *CalME*, a program that simulates pavement performance using a mechanistic-empirical approach. These inputs included data collected on traffic and environment, from condition surveys, and during falling weight deflectometer and material testing.

Two mainline flexible pavement cells—Cell 3 and Cell 21—were selected for the study for two reasons: because of the availability of material for laboratory testing by the UCPRC to characterize material response/performance models for *CalME* simulation, and because of the cells' contrasting pavement performance with respect to fatigue cracking and rutting.

For both cells, the *CalME* simulations, which presumed bottom-up fatigue cracking, matched reasonably well with the top-down cracking indicated by the condition survey. Whether the cracking resulted from a bottom-up or top-down process remains an open question.

CalME accurately predicted the rutting performance of Cell 3 appropriately; however, the rutting performance of Cell 21 did not match well with the software's predicted results, although possible over-asphalting during construction or the Marshall mix design might have contributed to premature rutting failure.

Overall, the use of *CalBack* and *CalME* for predicting pavement performance for this climate (cold winter, warm summer) appears promising. However, the *CalME* performance shift factor for rutting, developed from HVS testing, appears to need recalibration for normal traffic.

Keywords:
CalME, CalBack, fatigue cracking, rutting, mechanistic-empirical

Proposals for implementation:

Related documents:

Signatures

B.-W. Tsai **First Author**	J. Harvey, P. Ullidtz **Technical Review**	D. Spinner **Editor**	J. Harvey **Principal Investigator**	I. Basheer **Caltrans Technical Advisory Panel Tech Lead**	T. J. Holland **Caltrans Contract Manager**

DISCLAIMER

The contents of this report reflect the views of the authors, who are responsible for the facts and accuracy of the data presented herein. The contents do not necessarily reflect the official views or policies of the State of California, the State of Minnesota, or the Federal Highway Administration. This report does not constitute a standard, specification, or regulation.

PROJECT OBJECTIVES

The study presented in this tech memo is part of Partnered Pavement Research Center Strategic Plan Element 4.1 (PPRC SPE 4.1), whose objective is to evaluate and develop mechanistic-empirical design procedures for California. The study presented in this tech memo is a simulation of the performance of two sections of the Minnesota Road Research Project (Mn/ROAD) using the mechanistic-empirical analysis program *CalME,* and the deflection backcalculation program *CalBack,* and comparison with field results.

ACKNOWLEDGMENTS

The research associated with this paper was conducted as a part of the Partnered Pavement Research Program supported by the California Department of Transportation (Caltrans) Division of Research and Innovation. The contract managers were Dr. Joe Holland and Mr. Michael Samadian, and the program manager was Mr. Nick Burmas. The authors also wish to thank Minnesota Department of Transportation (MnDOT) for their support in providing comprehensive database and material for fatigue and shear testing. Special thanks go to Mr. Tim Clyne, Mr. Ben Worel, and Dr. Shongtao Dai of MnDOT.

TABLE OF CONTENTS

LIST OF FIGURES

LIST OF TABLES

1 INTRODUCTION

This study demonstrates how the software programs *CalBack* and *CalME* were used to predict the in-situ pavement performance of two test sections at the Minnesota Road Research Project (Mn/ROAD).

In recent years increased interest has developed in mechanistic-empirical pavement designs that involve traffic, environment, and material properties as inputs to determine the potential distresses for new pavements or existing pavements *CalME* is a mechanistic-empirical design program developed for new flexible pavement and rehabilitation in California *(1)*. *CalME* software includes the existing design R-value method of the California Department of Transportation (Caltrans), a simple mechanistic-empirical design procedure (Asphalt Institute Method), and an Incremental-Recursive Mechanistic-Empirical (IRME) analysis method in which the material properties of the pavement are updated in terms of damage as the simulation of the pavement life progresses. The IRME analysis method incorporates different mathematical models to describe the behavior of various materials and to predict pavement performance. Although it was developed for use in California, *CalME* can be applied in the cold regions, as in the case of the Mn/ROAD project.

CalBack (2), *CalME*'s companion program, is used to determine pavement layer moduli using deflection test data obtained from a falling weight deflectometer (FWD). The program iteratively searches an optimum set of layer moduli, minimizing the residual sum of squares between calculated and measured deflections at the sensors (geophones). The default modulus calculation approach in *CalBack* is based on the Odemark-Boussinesq method *(3)* with consideration of subgrade nonlinearity. Other stress/strain calculation methods, such as layered-elastic theory and the Kalman filter, are also available in the software. The backcalculated layer moduli are important inputs to *CalME*; moreover, the backcalculation results of long-term monitored FWD tests make it possible to evaluate the influence of freeze/thaw cycles, seasonal changes, the confining effects of overlying layers on subgrade and aggregate base modulus, and the effects of hardening and aging on the modulus of hot-mix asphalt (HMA).

The Mn/ROAD project is a full-scale pavement testing facility where trafficking of test sections started in 1994. It is located near Albertville, Minnesota (40 miles northwest of Minneapolis–St. Paul). Mn/ROAD consists of two road segments parallel to I-94: (1) a 3.5-mile mainline interstate roadway with two lanes; and (2) a 2.5-mile closed-loop, low-volume roadway. On the mainline interstate roadway, traffic is moved onto bypass lanes during test section construction and data collection, and moved back the traffic onto the test section lanes to provide traffic loading.

In this case study, two mainline flexible pavement test cells were considered, Cell 3 and Cell 21 (shown in Figure 1.1), both of which use the same asphalt binder, AC 120/150 (PG58-28) (the binder conversion was made according to test results) *(4)*, and the same mix design method, Marshall 50-blow mix design. The pavement structures of Cell 3 and Cell 21 were designed for 5- and 10-year design lives respectively. Cell 3 consists of a 0.525 ft (160 mm) hot-mix asphalt layer (HMA), 0.333 ft (102 mm) Class-5 sp. aggregate base (AB), 2.750 ft (838 mm) Class-3 sp. aggregate subbase (ASB), and clay subgrade (SG) with an "R" value of 12. Cell 21 includes a 0.658 ft (201 mm) HMA layer, 1.917 ft (584 mm) Class-5 sp. aggregate base, and the same clay subgrade as Cell 3. These cells were selected because (a) stored material from the original construction in 1994 was available for UCPRC use in laboratory testing to develop response/performance models for *CalME* simulations and (b) these two cells exhibited contrasting rutting and fatigue cracking performance *(5)*. The aggregate base and subbase layers of Cell 3 were combined into a single layer for both the *CalBack* backcalculation and *CalME* simulations.

Prior to conducting the *CalME* simulations, efforts were made (a) to determine the material response/performance models for asphalt-bound and unbound materials, (b) to determine the traffic axle-load spectra and axle count, and (c) to incorporate surface temperature into the *Enhanced Integrated Climatic Model (EICM)* database results used by *CalME*. The response/performance models for asphalt-bound materials included the modulus of the asphalt layer (master curve), fatigue damage to the asphalt layer, and permanent deformation—which are characterized using the flexural frequency sweep test, flexural fatigue test, and repeated simple shear test at constant height (RSST-CH), respectively—as well as the effects of hardening and aging—which are determined from FWD backcalculation results. The main response/performance models for unbound material are permanent deformation, the confining effects of overlying layers on stiffness, and freeze/thaw effects and seasonal changes for subgrade modulus. The permanent deformation model coefficients were experimentally determined from previous studies (*6*) and coefficients for the other two models were determined based on the FWD backcalculation results. Table 2.1 and Table 2.2 summarize the response/performance models and associated parameter coefficients used in the *CalME* simulation. It should be noted that the tabulated model coefficients are applicable only to the Mn/ROAD case study. The *CalME* manual also contains other response/performance models, such as those for reflection cracking and cemented base crushing and fatigue, which were not used for this study because they are not applicable to the materials in the test sections analyzed.

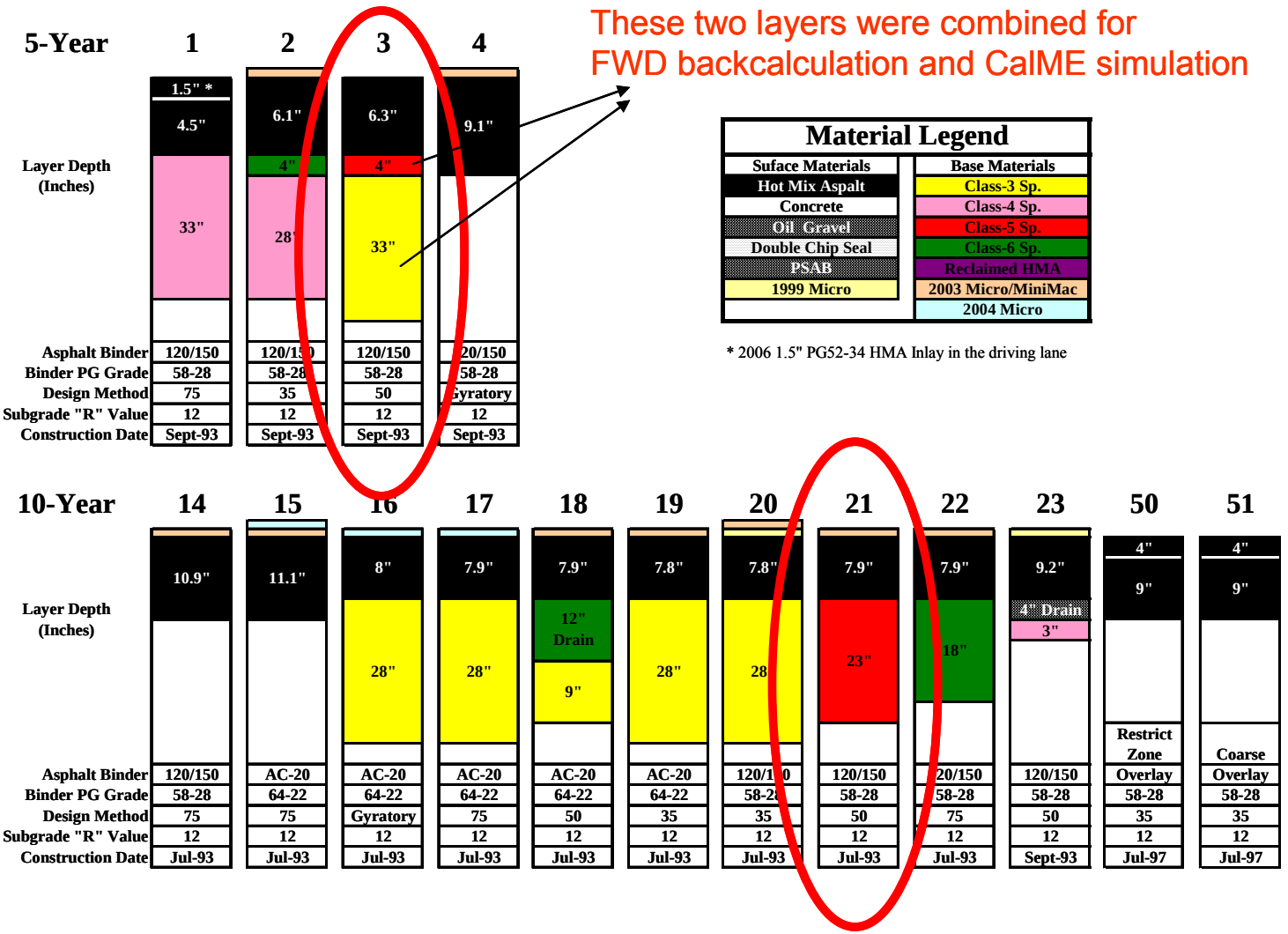

Figure 1.1: Two Mn/ROAD mainline HMA test sections, Cell 3 and Cell 21.
(Note: **The number in the Design Method row is the number of blows using the Marshall Design Method; "Gyratory" stands for Superpave Mix Design.)**

2 FWD BACKCALCULATION USING *CALBACK*

The Falling Weight Deflectometer (FWD) is widely used to characterize pavement response. A number of approaches are documented in the literature to backcalculate layer moduli by minimizing the difference between the measured surface deflections from the FWD and deflections calculated using a static model of the FWD load on a pavement characterized by layer elastic theory.

FWD data from long-term monitoring of the Mn/ROAD project provided a comprehensive database for *CalME* to evaluate the influence of freeze/thaw and seasonal changes, the confining effects of overlying layers, and changes in HMA stiffness. FWD testing was conducted at midlane (about 6.5 ft [2 m] off the left edge of the lane) and outer-wheelpath (about 9.8 ft [3 m] away from left edge of the lane) of both the truck and passing lanes. Each 500 ft (152 m) pavement test section included 10 stations spaced at 50-ft (15.2-m) intervals *(7)*.

The FWD backcalculated results conducted at the midlane and outer-wheelpath for both the truck and passing lanes were used to evaluate the freeze/thaw and seasonal changes effects for each cell. The confining effect of overlying layers on unbound materials moduli was evaluated using only the FWD backcalculated results at the outer-wheelpath of the driving lane of each cell. The midlane where FWD tests were conducted was assumed to have relatively minor traffic damage to the HMA; hence, the hardening/aging effect was evaluated with all the FWD backcalculated results obtained from the midlane results of both the truck and passing lanes for both test cells.

2.1 Freeze/Thaw and Seasonal Changes on Subgrade

Figure 2.1 presents an example of the FWD backcalculated layer moduli of Cell 21 at the outer-wheelpath, truck lane. It indicates a prominent annual periodic stiffness pattern and a noticeable freeze/thaw effect in the subgrade. To evaluate the annual freeze/thaw and seasonal changes effects on subgrade as input for *CalME,* the FWD backcalculated results were condensed into an equivalent one-year period, as shown in Figure 2.3(a) and Figure 2.3(b) for Cells 3 and 21, respectively. It should be noted that the backcalculated modulus variability was mainly due to the spatial variability over various stations. The results also show that the backcalculated modulus variability in cold weather is much more apparent than in warm weather. The backcalculated results from the small deflections measured in cold weather, when the HMA and frozen sub-grade are much stiffer, were susceptible to any small variations in deflection measurements from the sensors.

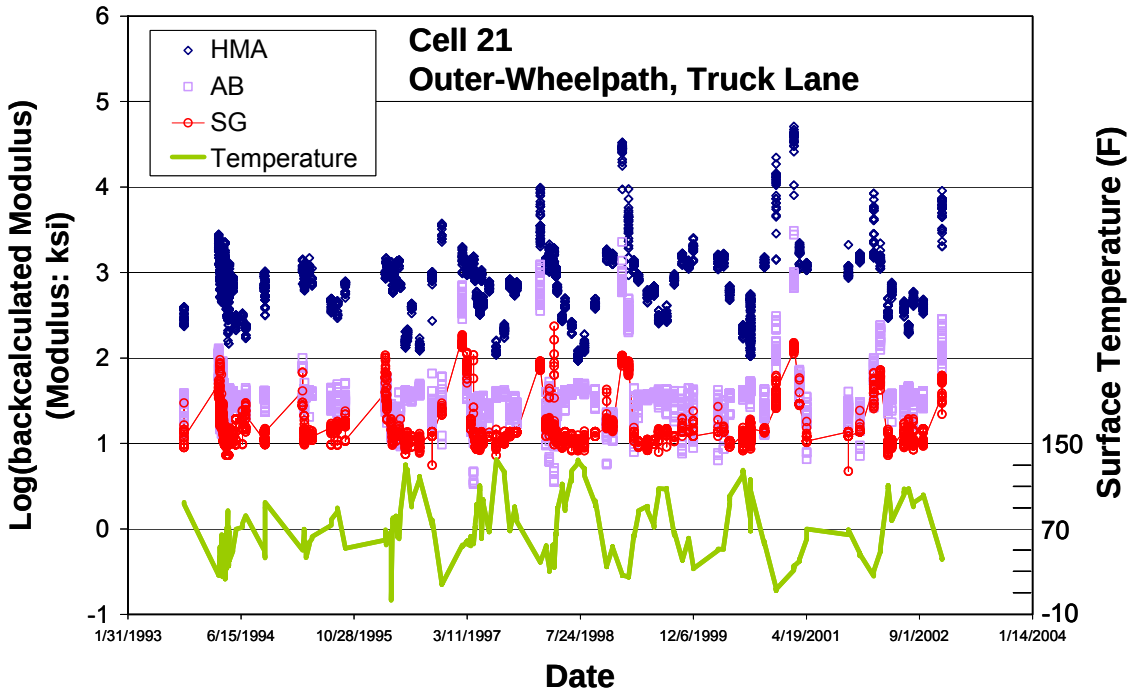

Figure 2.1: An example of the FWD backcalculated layer moduli and surface temperatures of Cell 21 at driving truck lane, outer-wheelpath.

Figure 2.2(a) schematically illustrates a model of the change of subgrade stiffness during freeze/thaw periods suggested by the Asphalt Institute (AI) in 1982 (*8*) that was used in this study to compare with the freeze/thaw subgrade modulus model currently included in *CalME*. The magnitude of duration and the rate of stiffness change vary depending on the temperature and rainfall, frost depth, groundwater condition, moisture content, subgrade soil, and possibly the pavement structure. Notice that the parameters in the AI model, T_{f0}, ΔT_f, ΔT_{ct}, ΔT_{rc}, ΔT_n, E_{fs}, E_{ns}, and E_{ts}, can uniquely define the subgrade modulus variations throughout the year. For convenience, t_1, t_2, t_3, t_4 (in terms of days rather than months) combined with E_{fs}, E_{ns}, and E_{ts} were used to conduct the model fitting. Two cases were considered in the AI model: (1) freeze started in spring (AI-spring, Figure 2.2[b]) and (2) freeze started in winter (AI-winter, Figure 2.2[c]). Figure 2.3(a) and Figure 2.3(b) also present the fitting results of both the *CalME* (Table 2.1 and Table 2.2) and AI-spring models for Cell 3 and Cell 21 respectively. Several observations can be made, as follows:

1. In general, the subgrade strength of Cell 3 is better than that of Cell 21 (based on either the magnitude of E_m or the difference between E_{fs} and E_{ts}). This might partly explain why Cell 3 has better rutting performance.
2. The fitting of AI-spring model shows that the timing of critical thaw is about 2 months after the beginning of the calendar year and it takes about 2.5 to 3.5 months for thaw recovery, i.e., until June or July.

3. Both the *CalME* and AI-spring models seem to describe the trend of stiffness variation appropriately. However, to retain the physical meaning of the recovery coefficient, *CalME* was subjected to certain constraints in the nonlinear fitting; as a result, the root-mean-squares (RMS) (or residual standard errors) of fittings were slightly higher than those using the AI-spring model (Cell 3: *CalME* [19.787] versus AI-spring [18.199]; Cell 21: *CalME* [16.975] versus AI-spring [13.940]).
4. The AI-winter model does not seem to describe the data appropriately even though the RMSs are slightly smaller than those of the AI-spring model. For this set of data, the fitting always leads to E_{fs} being equivalent to E_{ns}, which is not reasonable.
5. The *CalME* model seems to have a fitting trend that is the opposite of the backcalculated stiffnesses during the recovery stage, i.e., between days 150 and 250.

It seems that the AI-spring model provides a simple and realistic solution for the influence of freeze/thaw and seasonal changes on subgrade, and should be considered for inclusion in the *CalME* software.

2.2 Confining Effect on Aggregate Base Stiffness

It has been found that the moduli of unbound materials sometimes vary with the stiffnesses of the layers above them *(9).* A decrease in the stiffness of the layers above a granular layer would be expected to cause an increase in the bulk stress in the granular material and therefore, an increase in the modulus. However, results from several studies *(10,* for example) indicate that the opposite may often occur: as the stiffness of the overlying layers decreases the stiffnesses of the unbound layers also decrease. To allow for this effect, in *CalME* the stiffness of each unbound layer was modeled as a function of the bending stiffnesses of the layers above it. The stiffness of the unbound layer was simultaneously modeled as a function of load level using the well-known nonlinearity model, $\left(P/40\,\mathrm{kN}\right)^{\alpha}$.

In this study, α was set at 0.6. Notice that in the *CalME* model for confining effect (Table 2.1), *E* stands for the backcalculated modulus from FWD tests. Also, only the aggregate base layer was considered to have the confining effect. Figure 2.4(a) and Figure 2.4(b) illustrate the *CalME* model-fitting results for Cells 3 and 21, respectively. The higher moduli of the aggregate base, caused by variation of backcalculated results, seem to be the influential points that determine the fitting.

From the coefficients obtained from fitting, it can be found that if $S/S_{ref} > 0.3025$, then the calculated modulus of Cell 3 is greater than that of Cell 21; if $S/S_{ref} < 0.3025$, then it is the other way around. That is to say, most of the time, the modulus of the aggregate base in Cell 3 is greater than that of Cell 21 and this might suggest that

Cell 3 will produce less shear stress on top of the subgrade layer and less tensile strain at the bottom of the HMA layer when compared with Cell 21.

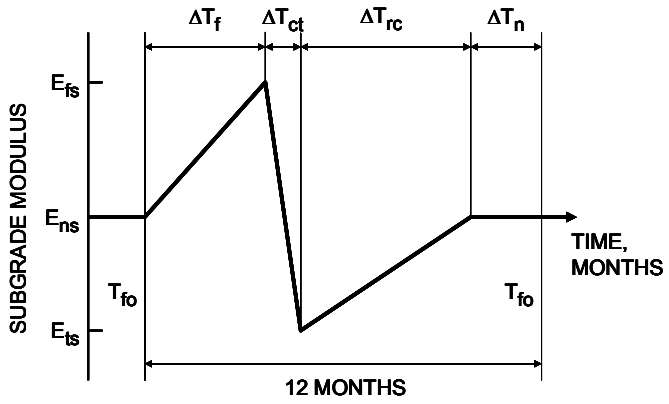

$E_{ts} = r_t \times E_{ns}$ — T_{fo} = Month freeze started

r_t = Thaw reduction factor — ΔT_f = Time of freeze

E_{ns} = Normal subgrade modulus — ΔT_{ct} = Time of critical thaw

E_{fs} = Frozen subgrade modulus — ΔT_{rc} = Time of thaw recovery

E_{ts} = Thaw (reduced) subgrade modulus — ΔT_n = Time-normal subgrade condition

(a) Asphalt Institute Frost/Thaw Relationship

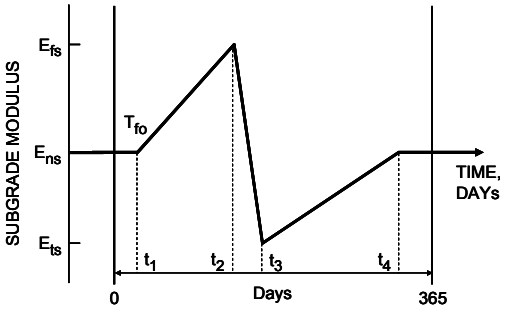

(b) Freeze Started in Spring

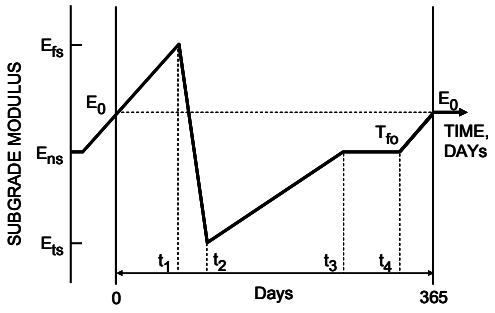

(c) Freeze Started in Winter

Note:
1. Parameter estimated: t_1, t_2, t_3, t_4, E_{fs}, E_{ns}, and E_{ts}.
2. E_0 is a function of t_1, t_4, E_{fs}, and E_{ns}.

Figure 2.2: Representation of subgrade modulus variations throughout year *(8):* (a) Asphalt Institute freeze/thaw relationship, (b) freeze started in spring, and (c) freeze started in winter.

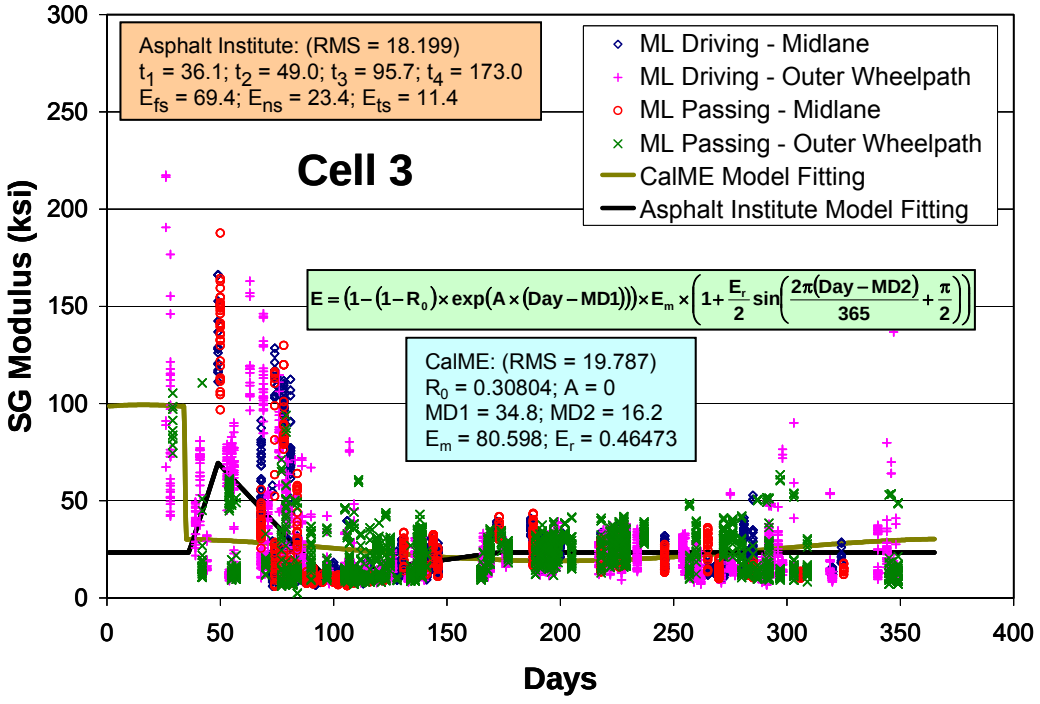

(a)

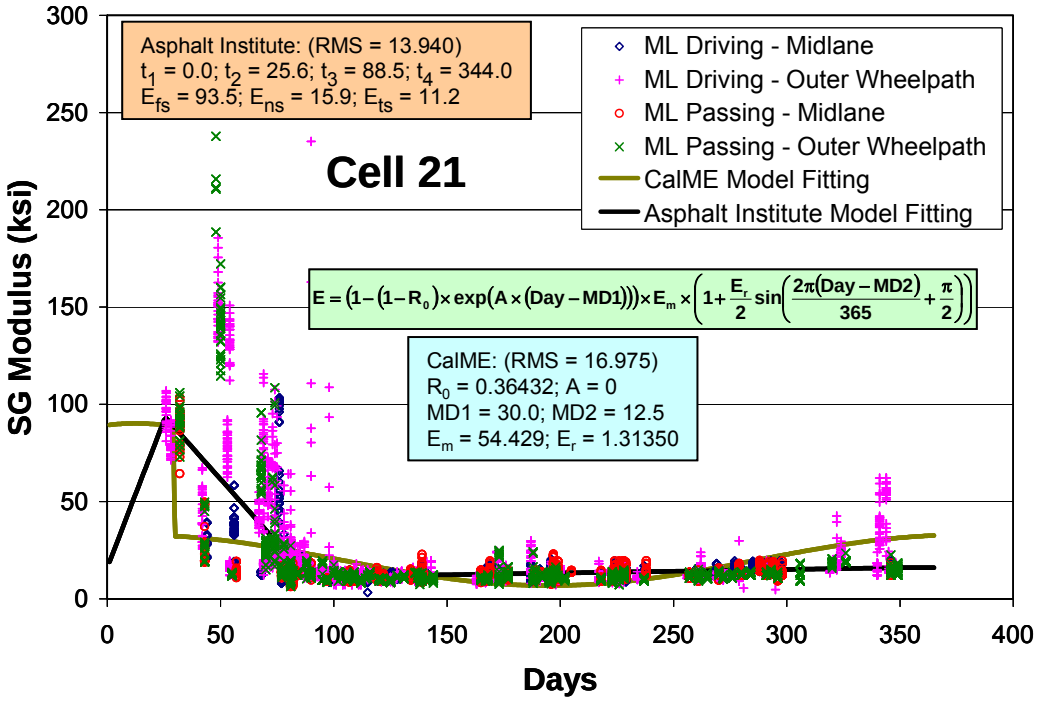

(b)

Figure 2.3: The influence of freeze/thaw and seasonal changes on subgrade with model fitting results: (a) Cell 3 and (b) Cell 21.

Table 2.1: *CalME* Response/Performance Models

	Response/ Performance Models	Testing/ Calculation Methods	Model Formulation	Model Parameter Definition
Asphalt-Bound Material	Modulus of Asphalt Layer (Master Curve)	Laboratory Flexural Frequency Sweep Test	$\log(E) = \delta + \frac{\alpha}{1+\exp(\beta+\gamma\log(tr))}$ $tr = lt \times \left(\frac{visc_{ref}}{visc}\right)^{aT}$ $\log(\log(visc\ \text{cPoise})) = A + VTS \times \log(t\ ^{\circ}K)$	E is modulus in MPa, tr is reduced time in sec, logarithms are to base 10, lt is loading time in sec, $visc_{ref}$ is binder viscosity at reference temperature, $visc$ is binder viscosity at present temperature, t is Kelvin temperature, and α, β, λ, δ, aT, A, and VTS are constants.
	Damage to Asphalt Layer	Laboratory Flexural Fatigue Test	$\log(E) = \delta^* + \frac{\alpha^* \times (1-\omega)}{1+\exp(\beta^* + \gamma^* \log(tr))}$ $\omega = \left(\frac{MN}{\phi \times MN_p}\right)^{\alpha} \qquad \alpha = \exp\left(\alpha_0 + \alpha_1 \times \frac{t}{1^o C}\right)$ $MN_p = A \times \left(\frac{\mu\varepsilon}{\mu\varepsilon_{ref}}\right)^{\beta} \times \left(\frac{E}{E_{ref}}\right)^{\gamma} \times \left(\frac{E_i}{E_{ref}}\right)^{\delta}$	α^*, β^*, λ^*, and δ^* are constants from master curve. ω is damage, MN is number of load applications in millions, $\mu\varepsilon$ is tensile strain at bottom of asphalt layer, E is damaged modulus, E_i is intact modulus, t is temperature, ϕ is shift factor that will be determined, and A, α, α_0, α_1, β, γ, δ, $\mu\varepsilon_{ref}$, and E_{ref} are constants.
	Permanent Deformation	Laboratory Shear (RSST-CH) Test	$rd_{AC} = K \times \gamma_i \times h$ $\gamma_i = \exp\left(A + \alpha \times \left[1 - \exp\left(-\frac{\ln(N)}{\gamma}\right) \times \left(1 + \frac{\ln(N)}{\gamma}\right)\right]\right) \times \exp\left(\frac{\beta \times \tau}{\tau_{ref}}\right) \times \gamma_e^{\delta}$	rd_{AC} is vertical rut depth in AC (mm), γ_i is permanent shear strain at 50 mm depth, K is a value relating permanent shear strain to rut depth, h is thickness of AC layer in mm, γ_e is corresponding elastic shear strain, N is equivalent number of load repetitions, and A, α, β, γ, δ, and τ_{ref} are constants.
	Hardening/Aging Effect	FWD Backcalculation	$E(d1) = E(d0) \times \frac{AgeA \times \ln(d1) + AgeB}{AgeA \times \ln(d0) + AgeB}$	$E(d)$ is modulus after d days, and $AgeA$ and $AgeB$ are constants.
	Crack Initiation	Experimentally Determined	$\omega_{initiation} = 1/\left(1 + \left(h_{HMA}/h_{ref}\right)^a\right)$	$\omega_{initiation}$ is fatigue damage when crack occurs, h_{HMA} is HMA thickness, h_{ref} is reference HMA thickness, and a is a constant.
Unbound Layer Material	Permanent Deformation	Experimentally Determined	$d_p = A \times MN^{\alpha} \times \left(\frac{\varepsilon}{\varepsilon_{ref}}\right)^{\beta} \times \left(\frac{E}{E_{ref}}\right)^{\gamma}$	d_p is permanent deformation (mm), MN is number of load repetitions in millions, and A, α, β, γ, ε_{ref}, and E_{ref} are constants.
	Confining Effect	FWD Backcalculation	$E = \left(\frac{P}{40\,kN}\right)^{\alpha} \times E_{ref} \times \left(1 - \left(1 - \frac{S}{S_{ref}}\right) \times Stiffness\_factor\right)$ $S = \left(\sum_1^{n-1} h_i \times \sqrt[3]{E_i}\right)^3$	E_{ref} is modulus (of layer n) at the reference stiffness, P is load level in kN, S is combined stiffness of layers above layer n, S_{ref} is the reference stiffness (=3500^3 N-mm), h_i is the thickness of layer i (mm), and α, E_{ref}, and $Stiffness\_factor$ are constants.
	Seasonal Changes and Freeze/Thaw Effect	FWD Backcalculation	$E = \underbrace{\left(1 - (1 - R_0) \times \exp(A \times (day - MD_1))\right)}_{\text{Frost/Thaw}} \times \underbrace{E_m \times \left(1 + \frac{E_r}{2} \sin\left(\frac{2\pi(day - MD_2)}{365} + \frac{\pi}{2}\right)\right)}_{\text{Seasonal\_Changes}}$	$R = 1 - (1 - R_0) \times \exp(A \times (day - MD_1))$ is the recovery coefficient, $MaxDay$ is the day with maximum stiffness, and R_0, A, E_m, E_r, MD_1 and MD_2 are constants.

Note: The SI-unit-only version 20080701 of *CalME* was used at the time the report was written.

Table 2.2: Coefficients for *CalME* Response/Performance Models

	Response/ Performance Models	Model Formulation	Model Parameter Definition	
Asphalt-Bound Material	Modulus of Asphalt Layer (Master Curve)	$\log(E) = \delta + \frac{\alpha}{1+\exp(\beta+\gamma\log(tr))}$ $tr = lt \times \left(\frac{visc_{ref}}{visc}\right)^{aT}$ $\log(\log(visc\ \text{cPoise})) = A + VTS \times \log(t\ ^{o}K)$	Cell 3 and Cell 21	
			δ = 2.30103	A = 9.6307
			α = 1.739885	VTS = -3.5040
			β = 0.379806	E_{ref} = 3739
			γ = 0.756055	T_{ref} = 20
			aT = 1.120961	
	Damage to Asphalt Layer	$\log(E) = \delta^{*} + \frac{\alpha^{*}\times(1-\omega)}{1+\exp(\beta^{*}+\gamma^{*}\log(tr))}$ $\omega = \left(\frac{MN}{\phi \times MN_p}\right)^{\alpha}$ $\alpha = \exp\left(\alpha_0 + \alpha_1 \times \frac{t}{1^{o}C}\right)$ $MN_p = A \times \left(\frac{\mu\varepsilon}{\mu\varepsilon_{ref}}\right)^{\beta} \times \left(\frac{E}{E_{ref}}\right)^{\gamma} \times \left(\frac{E_i}{E_{ref}}\right)^{\delta}$	Cell 3 and Cell 21	
			δ^{*} = 2.30103	A = 120.972001
			α^{*} = 1.739885	β = -1.35767
			β^{*} = 0.379806	γ = -0.67883
			γ^{*} = 0.756055	δ = 0
			α_0 = -1.18612	E_{ref} = 3000
			α_1 = 0	$\mu\varepsilon_{ref}$ = 200
			ϕ = 3.0	
	Permanent Deformation	$rd_{AC} = K \times \gamma_i \times h$ $\gamma_i = \exp\left(A + \alpha \times \left[1 - \exp\left(-\frac{\ln(N)}{\gamma}\right) \times \left(1 + \frac{\ln(N)}{\gamma}\right)\right]\right) \times \exp\left(\frac{\beta \times \tau}{\tau_{ref}}\right) \times \gamma_e^{\delta}$	Cell 3 and Cell 21	
			A = 0.992354	δ = 1
			α = 4.126821	τ_{ref} = 0.1
			γ = 2.675362	K = 1.4
			β = 0	
	Hardening/Aging Effect	$E(d1) = E(d0) \times \frac{AgeA \times \ln(d1) + AgeB}{AgeA \times \ln(d0) + AgeB}$	Cell 3 and Cell 21	
			$E(d0)$ = 2500	$AgeB$ = 1
			$AgeA$ = -0.26	
	Crack Initiation	$\omega_{initiation} = 1/\left(1 + \left(h_{HMA}/h_{ref}\right)^{a}\right)$	Cell 3 and Cell 21	
			h_{ref} = 250 mm	a = -2.0
Unbound Layer Material	Permanent Deformation	$d_p = A \times MN^{\alpha} \times \left(\frac{\varepsilon}{\varepsilon_{ref}}\right)^{\beta} \times \left(\frac{E}{E_{ref}}\right)^{\gamma}$	Cell 3 and Cell 21	
			Aggregate Base	Subgrade
			A = 0.8	A =1.1
			α = 0.3333	α = 0.3333
			β = 1.3333	β = 1.3333
			γ = 0.3333	γ = 0.3333
			ε_{ref} = 1000	ε_{ref} = 1000
			E_{ref} = 40	E_{ref} = 40
	Confining Effect	$E = \left(\frac{P}{40\,kN}\right)^{\alpha} \times E_{ref} \times \left(1 - \left(1 - \frac{S}{S_{ref}}\right) \times Stiffness\_factor\right)$ $S = \left(\sum_{1}^{n-1} h_i \times \sqrt[3]{E_i}\right)^{3}$	Cell 3	Cell 21
			α = 0.6	α = 0.6
			E_{ref} = 321.139	E_{ref} = 200.83
			$Stiffness\_factor$ = 0.840452	$Stiffness\_factor$ = 0.485041
	Seasonal Changes and Freeze/Thaw Effect	$E = \underbrace{\left(1 - \left(1 - R_0\right) \times \exp\left(A \times \left(day - MD_1\right)\right)\right)}_{\text{Frost/Thaw}} \times$ $\underbrace{E_m \times \left(1 + \frac{E_r}{2} \sin\left(\frac{2\pi\left(day - MD_2\right)}{365} + \frac{\pi}{2}\right)\right)}_{\text{Seasonal\_Changes}}$	Cell 3	Cell 21
			R_0 = 0.30424	R_0 = 0.36432
			A = 0	A = 0
			MD_1 = 28.6	MD_1 = 28.6
			MD_2 = 15.8	MD_2 = 12.5
			E_m = 565.584	E_m = 375.276
			E_r = 0.48242	E_r = 1.31350

Notes: 1.The SI-unit-only version 20080701 of *CalME* was used at the time the report was written.
2. The tabulated model coefficients are applicable only to the Mn/ROAD case study.

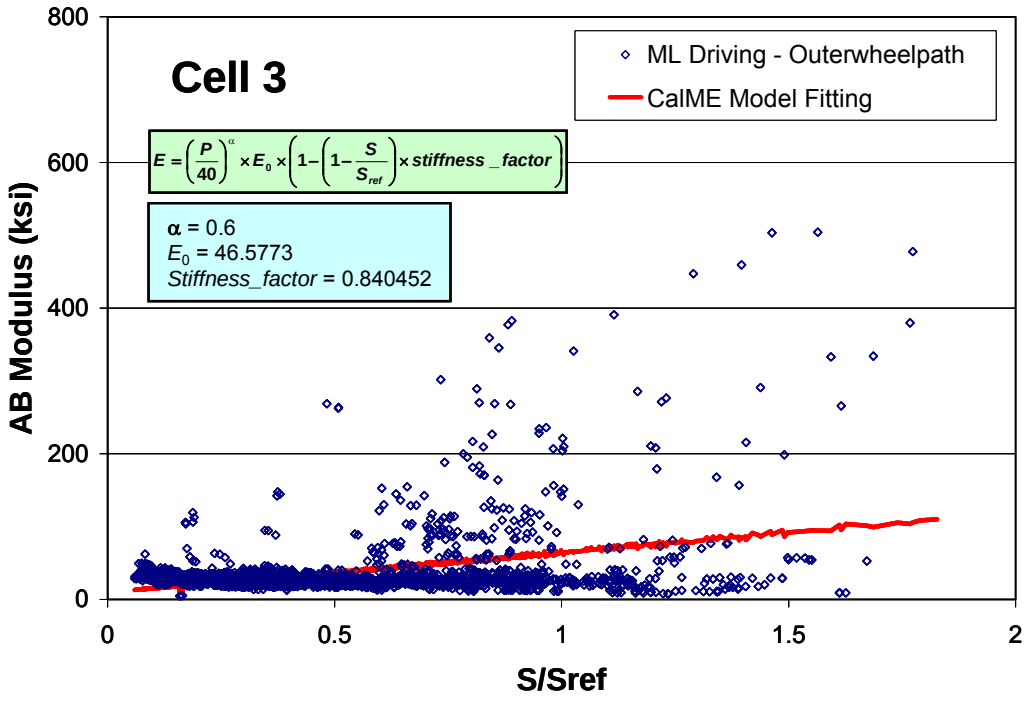

(a)

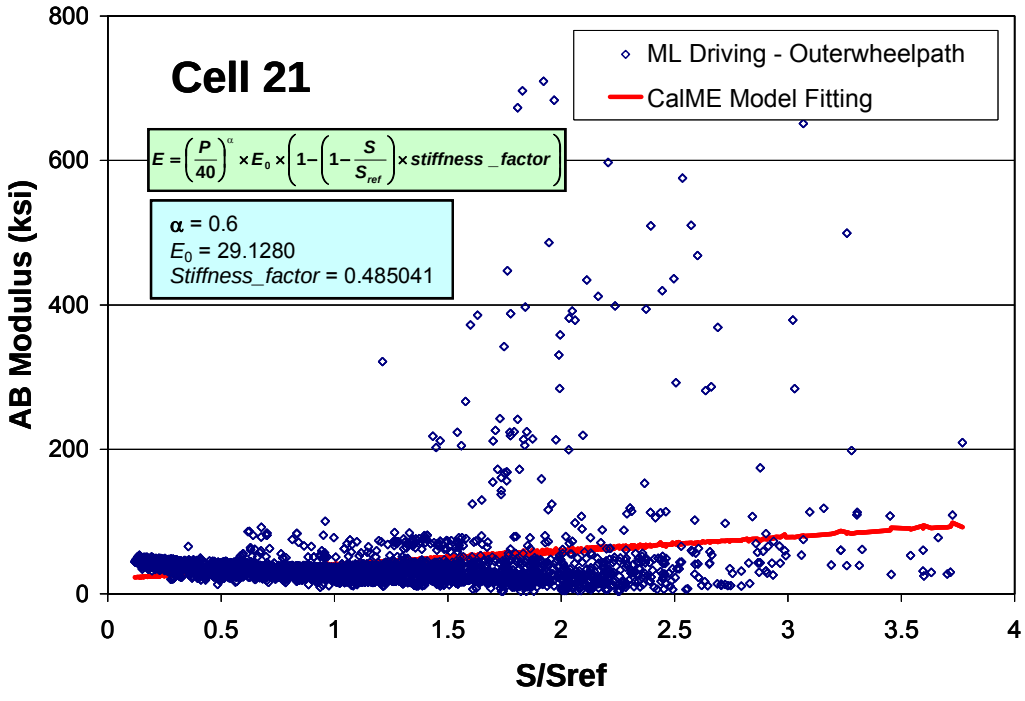

(b)

Figure 2.4: The confining effect on aggregate base with model fitting results: (a) Cell 3 and (b) Cell 21.

2.3 Hardening/Aging Effect on HMA

For an HMA mix, hardening refers to the loss of volatile components in heated asphalt during the construction phase (short-term aging); aging refers to the progressive oxidation of the in-place material (long-term aging) *(11).* The increase of viscosity due to hardening causes the mix to become stiff and brittle; as a consequence, it is susceptible to low-temperature cracking and fatigue cracking. However, the aging will normally increase the mix stiffness and thus reduce the shear stress/strain in the HMA layer making it more rutting-resistant.

The hardening/aging effect on HMA has long been recognized by pavement engineers. It is also known that FWD data from long-term monitoring is required to evaluate the hardening/aging effect on the AC layer, alone or in combination with coring and mix stiffness testing in the laboratory. The FWD data collected from the Mn/ROAD project provides the opportunity to assess the aging model. To prevent confounding between hardening/aging and traffic-induced damage, the FWD data conducted at midlines between the wheelpaths, which were considered to have minor traffic damage, was used to develop the aging model.

Figure 2.5 presents the HMA stiffness backcalculation results and *CalME* model fitting (Table 2.1 and Table 2.2) as well. It should be noted that the temperature effect of the backcalculated HMA moduli was corrected using the master curve to a reference temperature of 68°F (20°C). The backcalculated results of each pavement test cell begin at the construction date of each cell. A smoothed line shows the possible trend of the aging model even though the modulus variation is considerable. It is apparent that most of the aging was completed in the first three years, and that no further aging was perceived afterwards. The aging pattern fit by the *CalME* model is in good agreement with the smoothed line; however, the *CalME* model cannot converge because increase of *AgeA* in the aging equation shown in Figure 2.5 will cause a concurrent increase of *AgeB*. As a result, the *AgeB* parameter was set to 1.0 so as to stabilize the fitting.

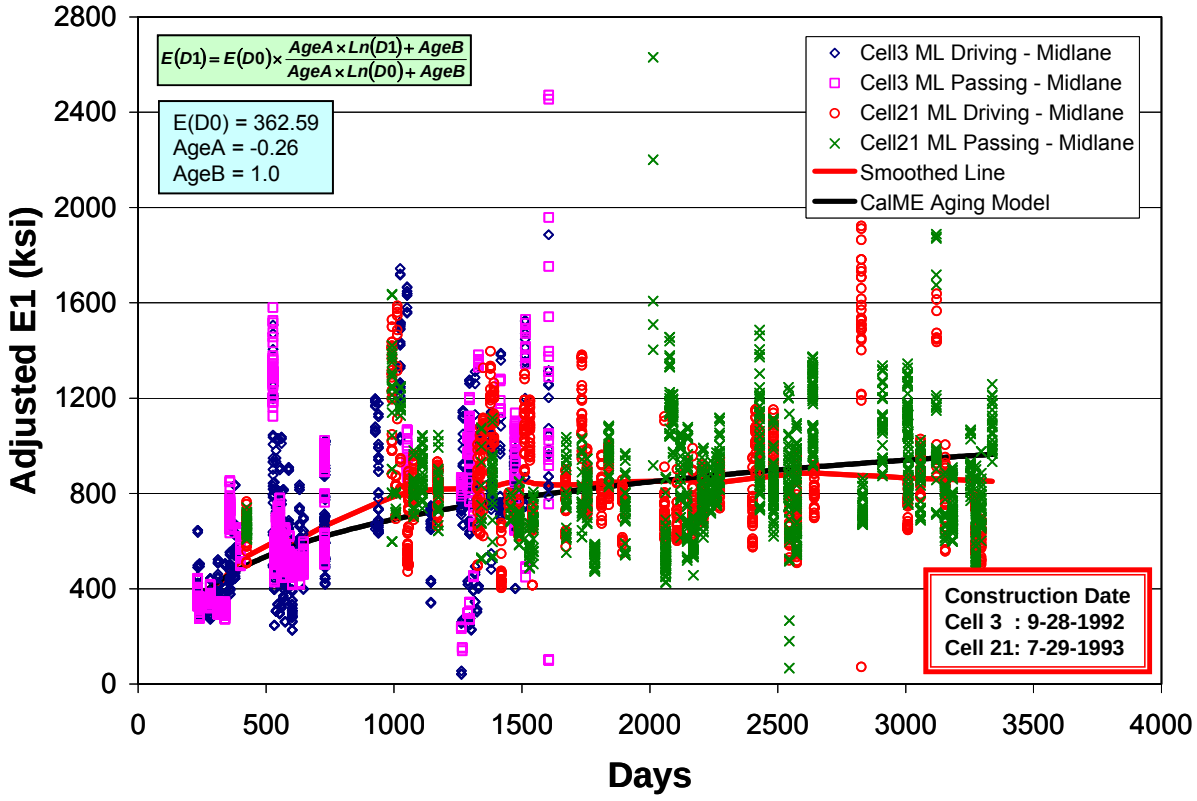

Figure 2.5: The aging effect on backcalculated HMA stiffness and associated model-fitting results.

3 DATA PREPARATION FOR *CALME* SIMULATION

Inputs required for conducting *CalME*-IRME simulation can be categorized as follows:

1. Pavement structure, including layer thickness and mechanical properties for each layer. The mechanical properties required are different for asphalt-bound and unbound materials. The asphalt-bound/unbound material response/performance models are shown in detail in Table 2.1.
2. Traffic axle-load spectra, traffic axle count, and truck growth rate.
3. Environment, mainly pavement temperatures through the asphalt-bound layers.
4. Pavement condition data, mainly fatigue cracking and rutting.

As discussed earlier, the use of FWD data from long-term monitoring makes it possible to evaluate the influence of freeze/thaw and seasonal changes on subgrade stiffness, the confining effect on aggregate base, and the hardening/aging effect on HMA. In addition, the required inputs include the pavement response/performance models for the unbound and HMA layers, the traffic and environment, and the pavement performance data.

3.1 Pavement Response/Performance Models for HMA

The primary response/performance models for HMA include the stiffness master curve, and models for fatigue damage and permanent deformation. Their associated parameters (Table 2.1 and Table 2.2) were determined using flexural frequency sweep tests (variation of AASHTO T321), flexural fatigue tests (AASHTO T321), and repeated simple shear tests with constant height (RSST-CH; AASHTO T320), respectively. To develop the master curve, the standard test plan consisted of six tests on beams: three temperatures (50, 68, 86°F [10, 20, 30°C]), one strain level (either 100 or 200 microstrain), and two replicates. The sequence of loading frequencies went from 15, 10, 5, 2, 1, 0.5, 0.2, 0.1, 0.05, 0.02, to 0.01 Hz (from quick to slow). The standard test plan for fatigue damage included 18 tests on beams: three temperatures (50, 68, 86°F [10, 20, 30°C]), two strain levels, and three replicates with a 10-Hz loading frequency. To characterize permanent deformation, the standard test plan included 18 tests on cores: two temperatures (113 and 131°F [45 and 55°C]), three stress levels (10.1, 14.5, and 18.8 psi [70, 100, and 130 kPa]), and three replicates. All the specimens were prepared using the loose mixes from Mn/ROAD test cells, which had 50-blow Marshall mix designs. All the specimen preparation and testing were conducted at the Richmond Field Station laboratory of the University of California Pavement Research Center (UCPRC), Davis and Berkeley. The loose mixes were compacted using rolling-wheel compaction. The percent air-void content was targeted at 6.5±0.5% for both fatigue and shear specimens. This percentage was determined from Mn/ROAD in-place density results. Loose mix shipped from Minnesota was reheated for two hours at 270°F (132°C) for compaction. One uncertainty in the results is the amount of aging of the in-place HMA materials versus the aging of the specimens reheated from loose mix and compacted in the laboratory. Some indication of differences between field and laboratory aging of specimens can be obtained by

comparing the backcalculated stiffness from the field with the measured flexural stiffness from the laboratory specimens. FWD loading time normally ranges from 0.02 to 0.03 seconds, which are equivalent to loading frequencies from 6 to 8 Hz. As can be seen from Figure 3.1(a), the laboratory flexural stiffnesses were in the approximate range of 435,000 to 507,000 psi (3,000 to 3,500 MPa). As illustrated in Figure 2.5, the adjusted stiffnesses of the HMA layer in the first year ranged from 290,000 to 580,000 psi (2,000 to 4,000 MPa). The flexural stiffness obtained from master curve seems to be consistent with the backcalculated stiffness from FWD measurements; however, there is some uncertainty in this comparison because there is some damage even in specimens taken from between the wheelpaths, and the boundary conditions were different between the field deflection test and flexural beam.

Figure 3.1(a) illustrates the master curve of dynamic modulus in terms of reduced time and the *CalME* model fitting results. As can be seen, the fitting is very acceptable. Figure 3.1(b) compares the fitted and measured normalized stiffness from flexural fatigue test results. As seen in Figure 3.1(b), a strong pattern appears around the equality line which might indicate that the Cobb-Douglas type of production function *(12)* used in the *CalME* fatigue damage model is not an appropriate model specification. The *CalME* model seems to underestimate fatigue damage when the stiffness ratio is less than 0.6. For higher temperatures, the inappropriate model specification in particular predicts less fatigue damage than it should, as demonstrated by the appearance of most of the high temperature testing curves above the equality line. Unlike the fatigue damage model, the permanent deformation model issued very satisfactory fitting results (as shown in Figure 3.1[c]). It was found that the shear specimens made by 50-blow Marshall mix design seem to have very poor rutting-resistance at all testing conditions.

In addition, in *CalME,* an experimentally-determined relationship (Table 2.1) among damage, thickness of the asphalt layers, and crack initiation was developed using California Heavy Vehicle Simulator (HVS) tests and WesTrack performance data *(13, 14*). The coefficients, a = -2 and h_{ref} = 250 mm were determined based on the performance of sections with the Fine Superpave mix and the Fine Plus Superpave mix of WesTrack project.

3.2 Traffic and Environment

The traffic inputs include the following components: traffic axle-load spectrum, traffic axle count, and truck growth rate. In *CalME,* the traffic axle-load spectrum is defined as the frequency over 24 hourly periods of a day and over different axle load categories for each axle type. The traffic axle count is the total number of truck axles accumulated in the first year of simulation. The yearly total axle count will then be evenly distributed over each day based on the traffic axle-load spectrum. By default, in *CalME* no seasonal or daily variation of traffic volume is considered, only the hourly variation; however, these types of traffic volume adjustment are possible in the software.

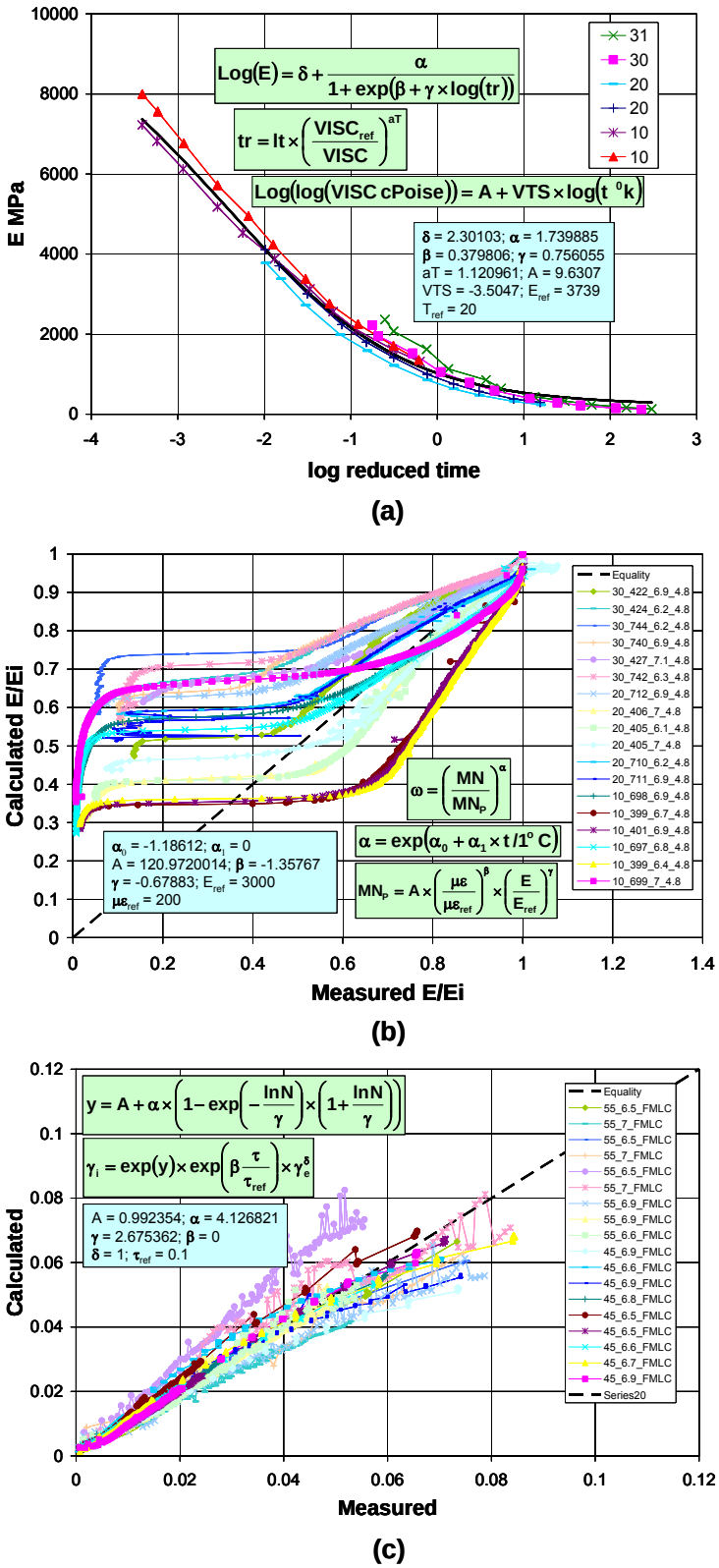

Figure 3.1: Pavement response/performance models and model-fitting results for HMA: (a) master curve, (b) fatigue damage to asphalt layer, and (c) permanent deformation.
***(Note:* The SI-unit-only version 20080701 of *CalME* was used at the time the report was written.)**

The original Mn/ROAD traffic data (1994 to 2008) was mainly organized by date, lane, truck class, and truck count. To prepare for *CalME* traffic input, the truck class and truck count had to be converted into axle type (steering, single, tandem, and tridem), axle load (ranging from 2,250 to 94,420 lbf [10 to 420 kN]), and axle count. Figure 3.2 presents the load spectra for different axle types. Notice that the load spectra of Figure 3.2 are only for the truck lane for which the simulation was conducted. The traffic is composed mainly of tandem (48.4 percent), steering (36.4 percent), and single (14.1 percent) axle types. Only 1.1 percent of traffic was composed of the tridem axle type at Mn/ROAD. The traffic axle count of the first year was about 1.45 million; the 5 percent truck growth rate was obtained from regression analysis after converting truck count to axle count. The total axle counts accumulated from 1994 to 2008 were about 8.7 million.

The environmental inputs mainly include pavement temperature and freeze/thaw on unbound layer modulus (as discussed in Section 2.1). *CalME* has a built-in database that contains hourly surface temperatures calculated using the EICM *(15)* using data from a 30-year period over a number of climatic zones and different pavement structures in California. During *CalME* simulation, pavement temperatures at different depths are calculated using surface temperature, a constant deep soil temperature, and previous temperatures. A 1-D Galerkin finite element formulation with a finite difference time step is used to complete the task. The Mn/ROAD surface temperatures were used to predict pavement temperatures of all depths in the HMA layer and incorporated into CalME EICM database. The Mn/ROAD surface temperatures were used to predict pavement temperatures of all depths in the HMA layer and incorporated into the *CalME EICM* database.

In *CalME,* there is no separate model for the effect of moisture content on subgrade; instead, the effect of moisture content was considered as part of seasonal changes on subgrade stiffness obtained from backcalculation of deflection data.

3.3 Pavement Condition Data

According to the condition report of Mn/ROAD *(5)*, the factors that affect the pavement performance of mainline HMA test cells include asphalt binder (PG58-28 versus PG64-22), mix design (35-, 50-, 75-blow Marshall and Gyratory), structure design (5-year versus 10-year design lives), aggregate base (5 base materials with varying thickness; drained and undrained subbase), traffic (truck and passing lanes), and environment (seasonal-temperature and moisture). In this case study, for Cell 3 and Cell 21 the differences mainly reside in structure design and aggregate base. Recall that the 5-year pavement structure of Cell 3 consists of HMA (0.525 ft [160 mm]), aggregate base (0.333 ft [102 mm]); Class-5 sp. per MnDOT specifications), and aggregate subbase (2.750 ft [838 mm]; Class-3 sp. per MnDOT specifications). The 10-year pavement of Cell 21 consists of HMA (0.658 ft [201 mm]) and aggregate base (1.917 ft [584 mm]; Class-5 sp.).

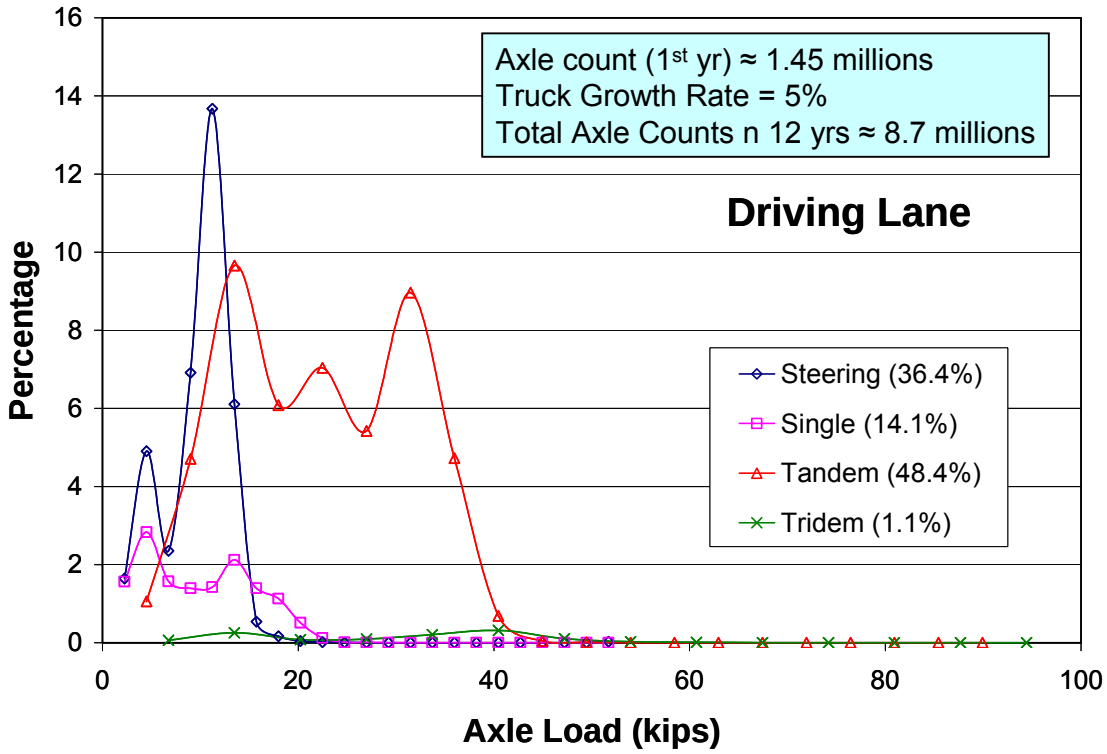

Figure 3.2: Traffic axle load spectra for truck lane.

This case study focuses only on fatigue cracking and rutting. A six-foot (1.829 m) straightedge (as shown in Figure 3.3) was primarily used to determine the maximum rut depth. It should be noted that the rut depth determined by the straightedge is defined as the distance from the top of the hump to the bottom of the wheelpath; the rut depth in *CalME* is downward rut only, not top to bottom. Figure 3.3 shows a cross section of the HMA rutting in a trench made in Cell 21 after trafficking. It can be seen that most of the rutting is in the top HMA lift which was 0.230 ft (70 mm) thick when originally constructed, with some additional rutting in the second lift which was 0.164 ft (50 mm) when constructed. Together, nearly all of the rutting occurred in the upper 20 mm of the HMA layer.

Investigators identified all the Mn/ROAD fatigue cracking as top-down cracking *(5)* with longitudinal surface-initiated cracks occurring in the wheelpaths: "The initial forensic core analysis has shown that these cracks are forming from the surface and moving downward. None of the forensic cores have shown the cracks to reach the bottom of the HMA surface." *(5)* The measurement "linear foot" along the wheelpaths of the truck lane was used as an index of fatigue cracking performance; the maximum amount of top-down cracking per cell is 1,000 linear feet, based on both wheelpaths at 500 linear feet (length of each test cell) each. To compare with the cracking performance predicted from *CalME,* the "linear foot" measurement was converted to "percent wheelpath cracking." *CalME* only simulates bottom-up cracking.

Figure 3.3: Photograph of the cross section of rutted HMA layer in trench in Cell 21 after trafficking.

Figure 3.4(a) and Figure 3.4(b), respectively, show the evolution curves of percent wheelpath cracking and rutting of Cells 3 and 21. The figures show that Cell 21 performed much better than Cell 3 in fatigue cracking, whereas Cell 21 performed much worse than Cell 3 in rutting. Note that year zero, the date from which the *CalME* simulation was initiated, is June 1994, the month the test facility opened to traffic.

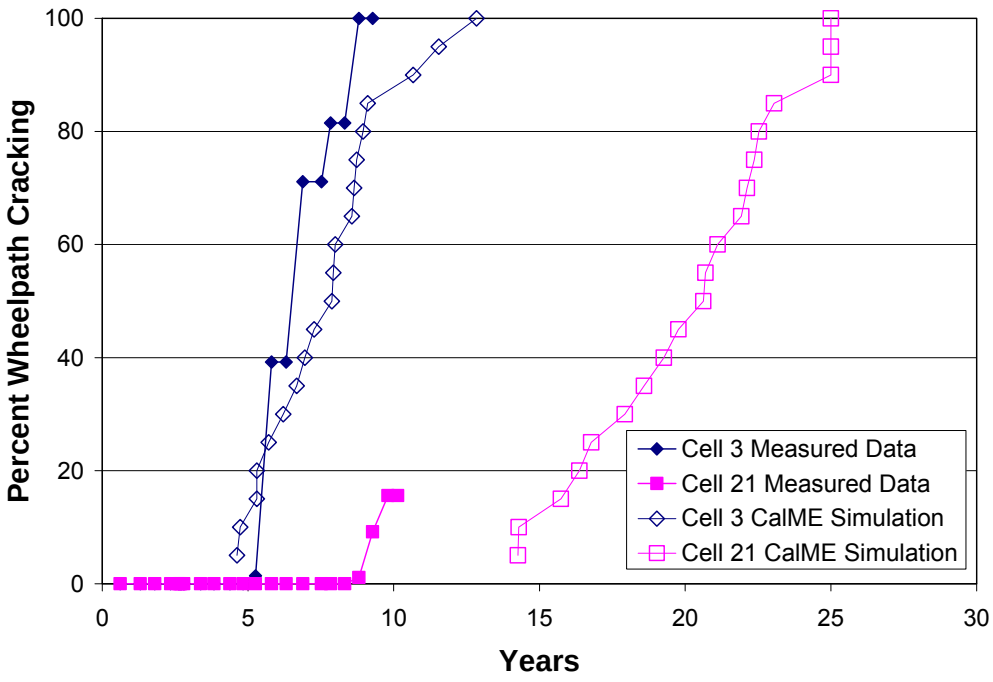

(a)

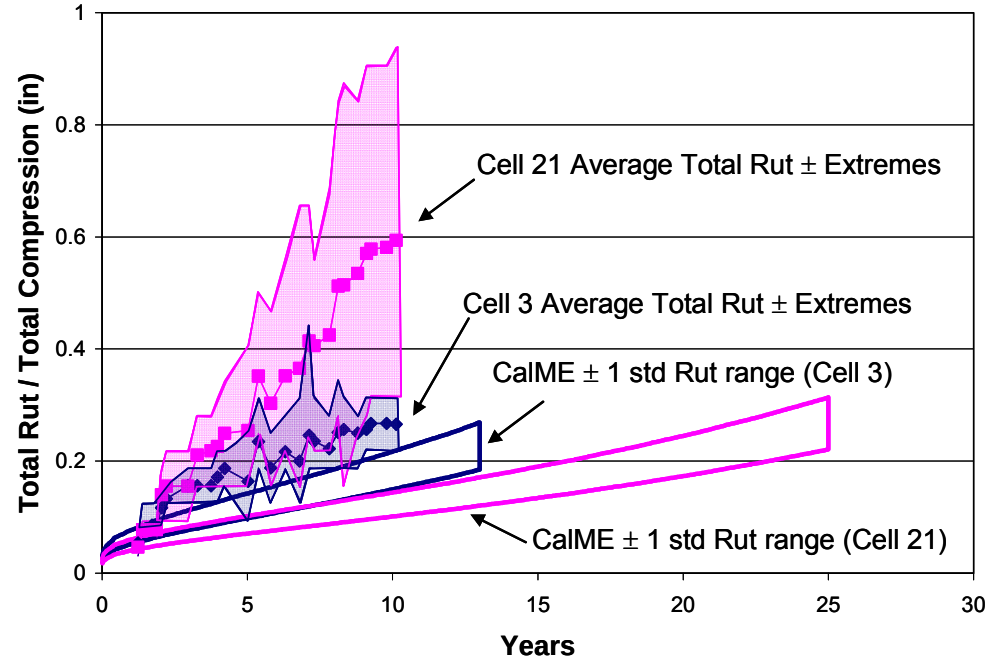

(b)

Figure 3.4: Mn/ROAD pavement condition data with *CalME* simulated results of Cell 3 and Cell 21: (a) fatigue cracking and (b) rutting. (Note: *CalME* simulates downward rut depth, Mn/ROAD measurements are total rut depth including humps at sides of wheelpath and downward rut in wheelpath)

4 PAVEMENT PERFORMANCE PREDICTION USING *CALME*

The *CalME*-IRME approach can be used for either deterministic or probabilistic analysis. In contrast to deterministic analysis, the probabilistic analysis takes into consideration construction variation in terms of layer thickness and layer stiffness, and laboratory material testing variation in terms of model parameters through the use of Monte Carlo simulation. The incorporation of traffic and environment variation through sensitivity analysis is currently under development in *CalME*. The primary objective in a Monte Carlo simulation is the generation of random numbers from known (or assumed) probability distributions for the selected variables; for a given set of generated random numbers, the simulation process is deterministic. The simulations become probabilistic when the distribution of results from the repeated simulations with the generated random number sets has been completed.

As noted previously, the distresses considered in this case study were fatigue cracking and rutting. As in the *CalBack* backcalculation, the aggregate base and subbase (AB and ASB) layers of Cell 3 were combined as a single layer when conducting the *CalME* simulations.

4.1 Fatigue Cracking

In the *CalME*-IRME approach, fatigue damage is assumed to be initiated at the bottom of the HMA layer and then propagated up to the surface as the simulation of pavement life progresses, i.e., the bottom-up fatigue cracking process. According to the Mn/ROAD condition survey report *(5),* the fatigue damage was all categorized as top-down cracking, which is completely contrary to the bottom-up cracking assumption in *CalME*. It is interesting to demonstrate whether the bottom-up fatigue cracking mechanism in *CalME* can probabilistically interpret/match the surface cracking patterns of Cell 3 and Cell 21 despite the observation from the Mn/ROAD report regarding the location of crack initiation (see Section 3.3).

The equation relating HMA damage level to surface cracking initiation, $\omega_{initiation} = 1/\left(1 + \left(h_{HMA}/h_{ref}\right)^{a}\right)$ (as tabulated in Table 2.1), is an experimental relationship associated with the thickness of the HMA layer based on California HVS tests and WesTrack experiments *(13, 14*) with h_{ref} = 250 mm and a = -2.0. Thus, the fatigue damage criterion that causes 5 percent surface cracking can be calculated as $\omega_{initiation}$ = 0.291 for Cell 3 (h_{HMA} = 0.525 ft [160 mm]) and $\omega_{initiation}$ = 0.393 for Cell 21 (h_{HMA} = 0.658 ft [201 mm]), which also illustrates how the $\omega_{initiation}$ criterion varies as the layer thickness varies due to construction variation. The fatigue damage performance model is responsible for the deterioration rate of HMA layer until it reaches $\omega_{initiation}$.

In *CalME,* variation was defined in two ways: (1) coefficient of variation (*CoV*), which is defined as standard deviation divided by the mean of a random number *X*, i.e., σ_X / μ_X and (2) standard deviation factor (*Sdf*) which is determined by the formulation $Sdf(X) = 10^{(SD\_of\_\log X)}$, where *X* is in log-normal distribution and *SD* is the standard deviation. The *CoV*s of layer thickness variation were set at 0.07, 0.1, and 0 for layers AC, AB, and SG respectively; the *Sdf*(modulus) was set at 1.15, 1.8, and 1.8 for the same respective layers. The *Sdf* (parameter A in permanent deformation equations) were all set at 1.2 for asphalt-bound layer and unbound layers; the *Sdf* (parameter *A* in fatigue damage equation) was set at 1.15 for the HMA layer. The shift factor applied to the HMA layer was 3.0, which is the number obtained from the calibration study from the California HVS tests *(13).*

Before interpreting the results of probabilistic analysis using Monte Carlo simulation, it is necessary to clarify the definition of the empirical cumulative distribution function, $F_n(x) = \frac{1}{n}(\#x_i \le x)$, where $F_n(x)$ gives the proportion of the data less than *x (16).* The *x* stands for the year in which surface cracking initiates in each subsection of the roadway corresponding to each Monte Carlo simulation for a given set of generated random numbers. In a sense, the various sets of random numbers generated from Monte Carlo simulation are conceptually equivalent to the spatial variation over the road section, with each simulation representing a subsection of the roadway length and crack initiation in each subsection representing failure of that incremental percentage of the wheelpath. Therefore, the probabilistic analysis using Monte Carlo simulation complies with the *linear foot* definition of fatigue cracking used in Mn/ROAD. For any given set of generated random numbers, the $\omega_{initiation}$ criterion and the associated fatigue damage response/performance model will determine the surface cracking progression associated with fatigue life. After completing all the sets of generated random numbers, the empirical cumulative distribution function, i.e., the fatigue cracking evolution curve, can be plotted. Figure 3.4(a) shows the *CalME*-predicted fatigue cracking evolution curves after 20 trials match reasonably well with the top-down cracking pavement condition data observed at Mn/ROAD. The question of the damage and progression of each crack remains open.

4.2 Rutting

As in the simulation of fatigue cracking, probabilistic analysis was applied in the rutting performance prediction for Cells 3 and 21. The same *CoV*s and *Sdf*s were used in the Monte Carlo simulation. The parameter coefficients for the permanent deformation response/performance models are tabulated in Table 2.2 for both the asphalt-bound and unbound materials. It should be noted that the parameter coefficients for the unbound materials were obtained from a pavement subgrade performance study conducted by the Federal Highway Administration in 1994 *(17)*. The total rut depth present on the surface in both the simulation and the observations in the field included not only deformation of the HMA layer, but also deformation from the

unbound layers. It was found that the rut deformation in the field had mostly formed in the upper lifts of the HMA layer rather than in the base or subgrade material *(4, 5).* The percentage of rut depth in each layer in the field was not available for comparison with the simulated rut depth in each layer as shown in Figure 4.1, and only the total rut depths were compared in this report.

From test results during the construction of the Mn/ROAD project *(4),* test Cells 3 and 21 (50-blow Marshall mix design) showed extracted asphalt contents of 5.6 percent and 5.9 percent by mass of mix (average of all lifts), respectively, which were 0.5 percent and 0.2 percent lower than the mix design recommendation of 6.1 percent. The extracted asphalt content of Cell 21 is 0.3 percent higher than that of Cell 3. Unfortunately, because the loose mix used to prepare the fatigue and shear specimens came from a different source than that of the two test cells, it is impossible to investigate performance differences due to the different as-built binder contents. There is therefore some uncertainty regarding the asphalt contents of the different lifts in the field and whether the loose mix used for laboratory specimens made for model parameter characterization was completely representative of the mix in the HMA layers in the field.

Figure 3.4(b) also presents the *CalME* simulation results after 20 trials of Monte Carlo simulation in terms of ± one standard deviation of rut range for Cell 3 and Cell 21. It should be noted that the applied shift factor $K = 1.4$ is also from the California HVS tests and WesTrack project *(13, 14*). It is possible to modify the shift factor K so that it matches the rutting evolution curve. The figure shows that *CalME* was able to predict the rutting performance of Cell 3 appropriately, although the rutting performance of Cell 21 was completely out of prediction even with a different definition of rutting. A higher possible asphalt content during construction of Cell 21 might partly explain this.

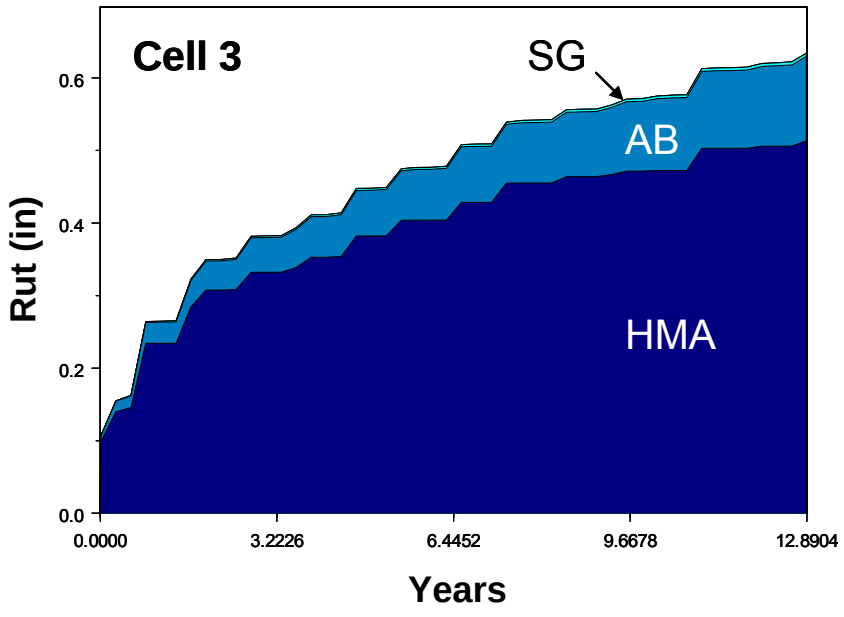

(a)

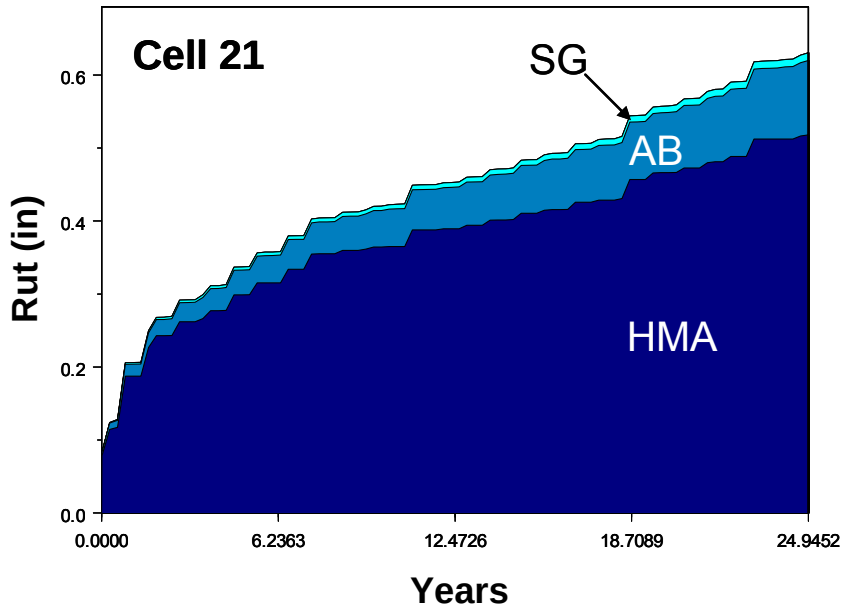

(b)

Figure 4.1: *CalME*-simulated rut depth in each layer: (a) Cell 3 and (b) Cell 21. (Note: *CalME* only simulates downward rut depth, while Mn/ROAD measurements of total rut depth include the humps at the sides of the wheelpath and the downward wheelpath rut depth.)

5 FINDINGS AND DISCUSSION

An attempt has been made to demonstrate the applicability of using *CalBack* and *CalME* in predicting the pavement performance in cold regions such as that of the Mn/ROAD case study. It should be emphasized that the applied shift factors for fatigue cracking and rutting were based on calibration studies from California Heavy Vehicle Simulator (HVS) tests and the WesTrack project. The shift factors could be modified to fit the pavement condition data better, but that was not done in this study. The following observations and suggestions are based on FWD backcalculation results using *CalBack* and pavement performance predictions of Mn/ROAD Cells 3 and 21 using *CalME*:

- *FWD data for modeling of long-term performance*: The FWD data from long-term monitoring provides a comprehensive understanding of the responses of materials subjected to the freeze/thaw cycle and seasonal changes of subgrade stiffness, the confining effect on stiffness of overlying layers, and the hardening/aging effect on HMA. *CalBack* offers an extremely practical and computationally efficient approach to backcalculating large amounts of deflection data.
- *Incremental-Recursive Mechanistic-Empirical Method*: The use of the IRME method in *CalME* provides insight into the pavement distress mechanisms as well as the final deterioration. Having the ability to predict the process of deterioration makes it possible to guarantee the initial investment cost and ensure that a pavement preservation strategy is launched in time.
- *Computation efficiency*: Due to incorporation of the precalculated *EICM* pavement temperature database, *CalME* is able to accelerate and improve computation efficiency significantly; for example, a 20-year simulation normally takes about 30 seconds for each run.
- *Monte Carlo Simulation*: The computational efficiency of *CalME* makes Monte Carlo simulation extremely practical. It took approximately 20 minutes to run 20 simulations. This computation speed makes it possible to investigate the influence of two construction/design variables—layer thickness and stiffness—on in-situ pavement performance. Reliance on the interpretation of the results of Monte Carlo simulations to match actual fatigue cracking seems to be more rational than relying on deterministic analysis.
- *Expandability of knowledge-based databases*: One of the significant features in *CalME* is the expandability of the knowledge-based databases. The *CalME* databases, including traffic, climate zone (temperature), and materials, are organized in such a way that engineers can add data for local materials, and can easily access and modify the databases as necessary to meet their specific requirements.

Although the benefits of using *CalBack* and *CalME* were demonstrated, there are still many improvements that can be made to them. Based on the use of *CalBack* and *CalME* in this case study, the following findings and suggestions are addressed:

- *FWD instrumentation and* CalBack: It was found that FWD instrumentation variation in winter will exaggerate the variation of *CalBack* backcalculation results. The magnitude of measured FWD deflection for the winter is much smaller than for the summer so, assuming that there is constant instrument variation, the result is a larger variation of backcalculated stiffness in winter.
- *Improved material response/performance models*: From this case study, it seems that the freeze/thaw model from the Asphalt Institute (AI) is more intuitive and simple to use compared with the current *CalME* model. Moreover, the AI model also had a better fit with the data. When fitting laboratory fatigue test results using *CalME* damage to the asphalt model, the Cobb-Douglas type of production function used to characterize the damage process did not match well with the propagation phase of the tests and might result in a conservative design. However, the surface crack initiation relation seems to be well justified. The new aging model in *CalME,* used for this case study, appeared to do a good job of predicting hardening/aging without needing any particular characterization with laboratory testing.
- *Considerations in Monte Carlo Simulation*: How to determine sampling size is a problem in using Monte Carlo simulation. Monte Carlo simulation is basically a sampling technique/process; as a consequence, the results are subject to a sampling error that decreases with increasing sample size. The sample size that issues the "exact" results has to be further evaluated.
- *Uncertainty in HMA laboratory specimens for model characterization*: There was some uncertainty regarding the binder contents of the HMA materials for both test sections, since the loose mix used to prepare laboratory specimens for laboratory testing for performance model characterization came from neither of the two test sections. In addition, the loose mix was reheated to prepare laboratory specimens, resulting in different aging than would have occurred in the field. For future case studies, it is recommended that field cores be taken from each test section for laboratory characterization.

REFERENCES

1. Ullidtz, P., J. T. Harvey, B.-W. Tsai, and C. L. Monismith. Calibration of Mechanistic-Empirical Models for Flexible Pavements Using California Heavy Vehicle Simulators. *In Transportation Research Board: Journal of the Transportation Research Board*, No. 2087, Transportation Research Board of the National Academies, Washington, D.C., 2008, pp. 20–28.
2. Lu, Q, P. Ullidtz, I. Basheer, K. Ghuzlan, and J. M., Signore. *CalBack*: Enhancing Caltrans Mechanistic-Empirical Pavement Design Process with New Backcalculation Software. *Journal of Transportation Engineering, ASCE*, Volume 135, Number 7, pp. 479–488, July 2009.
3 Ullidtz, P. Modeling Flexible Pavement Response and Performance. Polyteknisk Forlag, Oslo, Norway, 1998.
4 Stroup-Gardiner, M. and D. E. Newcomb. *Investigation of Hot Mix Asphalt Mixtures at Mn/ROAD*. Minnesota Department of Transportation. Report No. 97-06, February 1997.
5 Palmquist, D., B. Worel, and W. Zerfas. *2002 Mn/ROAD Hot-Mix Asphalt Mainline Test Cell Condition Report.* Office of Materials and Road Research, Minnesota Department of Transportation, Sep. 6, 2002.
6 Ullidtz, P. Simple Model for Pavement Damage. In *Transportation Research Board: Journal of the Transportation Research Board*, No. 1905. Transportation Research Board of the National Academies, Washington, D.C., 2005, pp. 128–137.
7 Cochran G., et. al. *Mn/ROAD Testing Protocols–Vol. 1*. Minnesota Department of Transportation, Report No. 97-22, December 1997.
8 The Asphalt Institute. Research and Development of the Asphalt Institute's Thickness Design Manual (MS-1) Ninth Edition. Research Report No. 82-2, August 1982.
9 Ullidtz, P., and P. Ekdahl. Full-Scale Testing of Pavement Response. *Proc., 5th International Conference on the Bearing Capacity of Roads and Airfields*, Vol. II, Trondheim, Norway, 1998.
10 Ullidtz, P., J. Harvey, B.-W. Tsai and D. Jones. Evaluation of Reflective Cracking Performance of AC Mixes with Asphalt Rubber Binder Using HVS Tests and Recursive Mechanistic-Empirical Analysis. *Proceedings, 6th RILEM International Conference on Cracking in Pavements,* Chicago, June 2008.
11 Bell, C. A. *Summary Report on Aging of Asphalt-Aggregate System*. SR-OSU-A-003A-89-2, Oregon State University, November 1989.
12 Named after C. W. Cobb and P. H. Douglas. See P. H. Douglas, *The Theory of Wages* (New York: Macmillan Co., 1934), pp. 132–135.
13 Ullidtz, P., J. T. Harvey, B.-W. Tsai, and C. L. Monismith. 2005. *Calibration of Incremental-Recursive Flexible Damage Models in CalME Using HVS Experiments*. Report prepared for the California Department of Transportation (Caltrans) Division of Research and Innovation by the University of California Pavement Research Center, Davis and Berkeley. UCPRC-RR-2005-06.
14 Ullidtz, P., J. T. Harvey, B.-W. Tsai, and C. L. Monismith. 2006. *Calibration of CalME Models Using WesTrack Performance Data*. UCPRC-RR-2006-14. Report prepared for Caltrans Division of Research and Innovation by University of California Pavement Research Center, Davis and Berkeley.
15 Larson, G. and B. Dempsey. *EICM Software. Enhanced Integrated Climatic Model Version 3.0 (EICM)*. Urbana, Illinois: University of Illinois, 2003.
16 Rice, J. A. *Mathematical Statistics and Data Analysis*. Wadsworth & Brooks/Cole Advanced Books & Software, 1988.
17 Federal Highway Administration. *Pavement Subgrade Performance Study, Plan of Work.* Final Report, FHWA, Washington, D.C., February 23, 1994.

APPENDIX A: LABORATORY FATIGUE/FREQUENCY SWEEP TEST RESULTS

Table A.1: Laboratory Flexural Frequency Sweep Test Results for Mixes of Mn/ROAD Project
(Three temperatures [10, 20, and 30°C]; two replicates)

MN219A2 (AV = 6.8%; 10°C)						MN284D1 (AV = 6.9%; 10°C)					
Freq (Hz)	Tensile Stress (MPa)	Tensile Strain	Flexural E* (MPa)	Phase Angle (deg)	Temp. (°C)	Freq (Hz)	Tensile Stress (MPa)	Tensile Strain	Flexural E* (MPa)	Phase Angle (deg)	Temp. (°C)
15.15	1.61066	0.000201	7994	18.4	9.80	15.15	1.43462	0.000199	7223	18.6	9.79
10.00	1.54079	0.000204	7559	17.5	9.79	10.00	1.37126	0.000201	6822	17.6	9.74
5.00	1.38784	0.000205	6766	17.7	9.78	5.00	1.24233	0.000203	6126	17.7	9.74
2.00	1.15231	0.000202	5718	18.2	9.75	2.00	1.04809	0.000202	5180	18.1	9.74
1.00	0.98560	0.000199	4947	19.7	10.11	1.00	0.90907	0.000201	4530	19.5	9.68
0.50	0.84347	0.000199	4232	22.2	10.02	0.50	0.77801	0.000200	3883	21.9	10.12
0.20	0.67047	0.000198	3379	25.3	9.85	0.20	0.62498	0.000200	3126	24.9	10.18
0.10	0.54778	0.000198	2761	28.7	9.70	0.10	0.51231	0.000200	2563	28.5	9.97
0.05	0.44620	0.000198	2249	32.1	9.88	0.05	0.42138	0.000200	2108	30.6	9.76
0.02	0.33817	0.000198	1707	33.9	9.96	0.02	0.32349	0.000200	1620	33.2	9.89
0.01	0.26802	0.000198	1354	35.3	9.90	0.01	0.26225	0.000200	1312	34.3	10.00
MN286D1 (AV = 6.9%; 20°C)						**MN2413C1 (AV = 6.0%; 20°C)**					
Freq (Hz)	Tensile Stress (MPa)	Tensile Strain	Flexural E* (MPa)	Phase Angle (deg)	Temp. (°C)	Freq (Hz)	Tensile Stress (MPa)	Tensile Strain	Flexural E* (MPa)	Phase Angle (deg)	Temp. (°C)
15.14	0.78978	0.000209	3778	31.9	19.98	15.20	0.86331	0.000210	4,108	31.0	19.93
9.96	0.66250	0.000196	3380	29.9	19.94	10.10	0.77514	0.000209	3,706	30.6	19.81
4.97	0.58743	0.000216	2720	30.4	19.81	4.97	0.64195	0.000214	3,005	29.5	19.94
1.99	0.42655	0.000215	1982	35.2	19.82	1.99	0.48223	0.000216	2,237	33.8	19.95
1.00	0.32271	0.000204	1585	35.9	19.93	1.00	0.36545	0.000204	1,794	34.7	19.83
0.50	0.24421	0.000201	1216	38.0	19.99	0.50	0.28515	0.000201	1,418	36.6	19.93
0.20	0.16940	0.000199	851	41.5	19.91	0.20	0.19884	0.000199	998	39.0	19.86
0.10	0.12524	0.000198	631	43.5	19.91	0.10	0.15066	0.000199	758	40.9	19.88
0.05	0.09443	0.000198	476	41.6	19.87	0.05	0.11264	0.000198	568	46.8	19.85
0.02	0.06259	0.000198	317	44.4	19.92	0.02	0.07491	0.000198	379	43.0	19.85
0.01	0.04685	0.000198	237	48.6	19.97	0.01	0.05827	0.000198	295	45.4	19.90
MN218D1 (AV = 6.8%; 30°C)						**MN285C1 (AV = 6.8%; 30°C)**					
Freq (Hz)	Tensile Stress (MPa)	Tensile Strain	Flexural E* (MPa)	Phase Angle (deg)	Temp. (°C)	Freq (Hz)	Tensile Stress (MPa)	Tensile Strain	Flexural E* (MPa)	Phase Angle (deg)	Temp. (°C)
15.14	0.49766	0.000223	2227	39.9	30.23	15.14	0.25563	0.000108	2363	38.7	31.55
10.00	0.41607	0.000213	1951	39.2	29.23	10.00	0.22594	0.000109	2068	37.5	30.81
5.00	0.32338	0.000213	1517	39.6	30.09	5.00	0.17640	0.000109	1621	38.3	31.57
2.00	0.21759	0.000207	1051	41.1	29.44	2.00	0.11854	0.000105	1128	39.3	30.23
1.00	0.15864	0.000202	784	42.1	29.71	1.00	0.08685	0.000102	855	39.8	31.44
0.50	0.11780	0.000201	586	43.2	29.63	0.50	0.06337	0.000099	642	42.7	30.29
0.20	0.07786	0.000199	392	45.2	29.72	0.20	0.04350	0.000100	435	43.9	30.22
0.10	0.05724	0.000199	287	46.0	29.87	0.10	0.03237	0.000099	327	44.6	30.62
0.05	0.04305	0.000199	217	45.9	29.58	0.05	0.02295	0.000098	235	43.3	30.73
0.02	0.02928	0.000197	149	44.3	29.67	0.02	0.01618	0.000098	164	45.8	30.76
0.01	0.02311	0.000198	117	45.0	29.60	0.01	0.01231	0.000097	127	39.4	30.69

Table A.2: Summary of Laboratory Flexural Controlled-Deformation Fatigue Test Results for Mixes of Mn/ROAD Project
(Three temperatures [10, 20, and 30°C]; two strain levels [400 and 700 microstrain]; three replicates; FMLC; AV = 6.5±0.5%; AC = unknown]

Specimen Designation	AV (%)	AC (%)	Test Temp. (°C)	Test Strain Level	Initial Phase Angle (Deg.)	Initial Stiffness (MPa)	Fatigue Life Nf
MN283C1	6.9		9.95	0.000400	19.87	6,547	809,074
MN284D2	6.7		9.97	0.000399	18.89	7,317	678,886
MN2412D2	6.4		9.98	0.000399	20.20	7,040	720,354
MN247C1	6.8		9.91	0.000694	22.22	6,308	43,448
MN286D2	6.9		9.92	0.000696	22.18	6,368	30,034
MN217C1	7.0		9.95	0.000694	21.13	6,795	10,625
MN281C2	6.1		20.02	0.000404	28.85	4,303	751,446
MN282D1	7.0		20.01	0.000403	25.56	5,186	519,148
MN2410D2	7.0		20.00	0.000405	36.43	3,258	644,052
MN218D2	6.9		19.90	0.000711	33.97	3,217	72,403
MN219A1	6.2		19.94	0.000706	33.84	3,464	55,506
MN285C2	6.9		19.91	0.000708	35.95	3,095	38,866
MN217C2	7.1		30.46	0.000427	46.95	1,614	278,008
MN248D2	6.2		30.33	0.000424	40.82	1,904	96,601
MN283C2	6.9		30.19	0.000422	44.02	1,715	856,988
MN215C1	6.3		30.59	0.000742	47.20	1,502	67,550
MN247C2	6.2		30.74	0.000742	46.69	1,507	62,142
MN2410D1	6.9		31.04	0.000741	43.83	1,734	48,387

APPENDIX B: LABORATORY SHEAR (RSST-CH) TEST RESULTS

Table B.1: Summary of Laboratory Shear (RSST-CH) Test Results for Mn/ROAD Mixes
(Two temperatures [45 and 55°C]; three stress levels [70, 100, and 130 kPa]; three replicates; FMLC; AV = 6.5±0.5%; AC = unknown]

Specimen Designation	AV (%)	AC (%)	Test Temp. (°C)	Test Shear Stress Level (kPa)	Initial Resilient Shear Modulus (MPa)	Permanent Shear Strain at 5,000 cycles	Cycles to 5% Permanent Shear Strain
34-MINII-10-1C-7045	6.9		44.92	74.69	156.5	0.083829	3,089
34-MINII-11-1D-7045	6.6		44.93	72.61	133.1	0.077441	3,225
34-MINII-11-2D-7045	6.9		45.23	71.92	111.3	0.150444	1,039
34-MINII-2-1D-10045	6.7		44.69	99.33	133.1	0.213269	1,000
34-MINII-6-2C-10045	6.6		44.67	97.47	106.2	0.242607	492
34-MINII-14-3C-10045	6.9		44.92	96.29	104.6	0.215501	555
34-MINII-6-1C-13045	6.5		44.90	127.47	100.6	0.276868	352
34-MINII-6-3C-13045	6.8		44.83	122.01	94.4	0.357881	242
34-MINII-11-3D-13045	6.5		45.25	126.18	115.1	0.319282	374
34-MINII-1-2C-7055	7.0		54.93	74.48	42.6	0.499182	95
34-MINII-7-3D-7055	6.5		54.79	67.14	53.9	0.322841	254
34-MINII-12-2C-7055	6.5		55.30	70.36	51.0	0.470001	190
34-MINII-2-3D-10055	6.9		54.86	86.92	43.3	0.425534	106
34-MINII-8-1C-10055	6.9		54.61	86.47	35.0	0.506258	62
34-MINII-10-2C-10055	6.6		54.93	86.47	40.4	0.450578	96
34-MINII-7-1D-13055	6.5		54.70	109.97	36.0	0.506258	91
34-MINII-8-2C-13055	7.0		54.89	110.86	NA	0.726639	29
34-MINII-12-3C-13055	7.0		55.40	114.26	38.1	0.620379	62